Heliyon 9 (2023) e22443

Contents lists available at ScienceDirect

Heliyon

journal homepage: www.cell.com/heliyon

Qi-Shen-Tang alleviates retinitis pigmentosa by inhibiting ferroptotic features via the NRF2/GPX4 signaling pathway

Meng Xiong [a,b], Chen Ou [c], Chang Yu [a,b], Jingyue Qiu [a,b], Jing Lu [d], Chaojun Fu [b,c], Qinghua Peng [c], Meiyan Zeng [b,**], Houpan Song [a,b,c,*]

[a] *Hunan Provincial Key Laboratory of Traditional Chinese Medicine Diagnostics, Hunan University of Chinese Medicine, Changsha, Hunan 410208, China*

[b] *School of Traditional Chinese Medicine, Hunan University of Chinese Medicine, Changsha, Hunan 410208, China*

[c] *Hunan Provincial Key Laboratory for Prevention and Treatment of Ophthalmology and Otolaryngology Diseases with Chinese Medicine, Hunan University of Chinese Medicine, Changsha, Hunan 410208, China*

[d] *School of Medicine, Hunan University of Chinese Medicine, Changsha, Hunan 410208, China*

ARTICLE INFO

Keywords:
Qi-Shen-Tang
Retinitis pigmentosa
NRF2
GPX4
ferroptosis

ABSTRACT

Ferroptosis has been observed during retinal photoreceptor cell death, suggesting that it plays a role in retinitis pigmentosa (RP) pathogenesis. Qi-Shen-Tang (QST) is a combination of two traditional Chinese medicines used for the treatment of ophthalmic diseases; however, its mechanism of action in RP and ferroptosis remains unclear. Therefore, this study aimed to explore the effect and potential molecular mechanisms of QST on RP. QST significantly improved tissue morphology and function of the retina in the RP model mice. A significant increase in retinal blood flow and normalization of the fundus structure were observed in mice in the treatment group. After QST treatment, the level of iron and the production of malondialdehyde decreased significantly; the levels of superoxide dismutase and glutathione increased significantly; and the protein expression of glutathione peroxidase 4 (GPX4), glutathione synthetase, solute carrier family 7 member 11, and nuclear factor erythroid 2-related factor 2 (NRF2) increased significantly. The molecular docking results demonstrated potential interactions between the small molecules of QST and the key proteins of NRF2/GPX4 signaling pathway. Our results indicate that QST may inhibit ferroptosis by inhibiting the NRF2/GPX4 signaling pathway, thereby reducing RP-induced damage to retinal tissue.

Abbreviations: DS, Danshen; ERG, Electroretinography; GPX4, Glutathione peroxidase 4; GQZ, Gouqizi; GSH, Glutathione; GSS, Glutathione synthetase; H&E, Hematoxylin and eosin; IOD, Integrated optic density; LSCI, Laser speckle contrast imaging; MDA, Malondialdehyde; NRF2, Nuclear factor erythroid 2-related factor 2; PUFA, Polyunsaturated fatty acids; QST, Qi-Shen-Tang; ROS, Reactive oxygen species; RP, Retinitis pigmentosa; SLC7A11, Solute carrier family 7 member 11; SOD, Superoxide dismutase; System xc-, Cystine/glutamate antiporter system; TCM, Traditional Chinese medicine; UPLC, Ultra-performance liquid chromatography.

* Corresponding author.Hunan Provincial Key Laboratory of Traditional Chinese Medicine Diagnostics, Hunan University of Chinese Medicine, 300 Xueshi Road, Yuelu District, Changsha, Hunan 410208, China.

** Corresponding author. School of Traditional Chinese Medicine, Hunan University of Chinese Medicine, 300 Xueshi Road, Yuelu District, Changsha, Hunan 410208, China.

E-mail addresses: xiongmeng@stu.hnucm.edu.cn (M. Xiong), ouchen@stu.hnucm.edu.cn (C. Ou), yuc@stu.hnucm.edu.cn (C. Yu), QiuJY@stu.hnucm.edu.cn (J. Qiu), 004026@hnucm.edu.cn (J. Lu), 004652@hnucm.edu.cn (C. Fu), 003450@hnucm.edu.cn (Q. Peng), 004324@hnucm.edu.cn (M. Zeng), songhp@hnucm.edu.cn (H. Song).

https://doi.org/10.1016/j.heliyon.2023.e22443
Received 23 February 2023; Received in revised form 9 November 2023; Accepted 13 November 2023
Available online 19 November 2023

1. Introduction

Retinal pigmentosa (RP) is a common retinal degenerative disease that causes vision loss due to the dysfunction and death of retinal photoreceptor cells, and usually affecting both eyes [1]. In the early stage of the disease, patients with RP usually experience night blindness. This is followed by progressive peripheral vision loss, visual field constriction, and eventual loss of central vision [2]. Globally, RP affects approximately 1.5 million individuals, presenting as an atypical retinal disease in approximately one in 4000 individuals [3]. Because of the irreversible blindness associated with RP and the rising incidence, early diagnosis and treatment are essential to delay disease progression and reduce the possibility of blindness.

Currently, the therapeutic regimes used for RP include medications, such as vitamin A [4] and neurotrophic factors therapy [5], gene therapy [6], and stem cell transplantation therapy [7]. Despite extensive studies and trials, currently available treatment approaches have several clinical limitations. First, there is no evidence that these drugs target the fundamental cause of RP, and their long-term safety and efficacy are yet to be comprehensively evaluated [8]. Second, because of the widespread heterogeneity of RP, gene therapy and stem cell transplantation are associated with high medical costs and risks [9]. Therefore, the development of more selective, safer, efficacious, and cost-effective treatments is necessary.

The benefits of traditional Chinese medicine (TCM) and natural plant extracts in the treatment of eye diseases have been demonstrated in many studies [10,11]. Qi-Shen-Tang (QST) is a TCM prescription comprising Gouqizi (GQZ) and Danshen (DS) at a ratio of 1: 1 that is used to reinforce deficiency and promote blood circulation. The clinical therapeutic effects of two Chinese herbal medicines that make up QST have been demonstrated in patients with RP [12,13]. However, the underlying therapeutic mechanisms of QST in RP remain unclear.

The scientific name for GQZ is *Lycium barbarum* L., which is the mature fruit of the Solanaceae plant, Gouqi. In addition to its sweet taste and neutral nature, GQZ has many pharmacological benefits, including invigoration of the liver and kidneys and enhancement of vision. Reports have shown that GDZ exhibits a wide range of biological activities, including antioxidant, anti-inflammatory, immunomodulatory, and neuroprotective functions [14,15]. Effective components of GQZ have been shown to promote photoreceptor survival, ameliorate retinal structure and function, and improve visual behavior in mice model and patients with RP [16–18]. The scientific name for DS is *Salvia miltiorrhiza* Bunge, which is the root of the Lamiaceae plant, Danshen. In addition to its bitter taste and slightly cold nature, DS has many pharmacological benefits as an important TCM herb dating back thousands of years, including the activation of blood circulation and elimination of stasis. Several water-soluble phenol-rich antioxidant compounds are extracted from DS, and these compounds can protect retinal pigment epithelium cells by preventing lipid peroxidation and inhibiting malondialdehyde formation [19,20]. Our previous studies [21,22] demonstrated that the QST extract improves both the morphology and function of the retina.

However, the molecular pathogenesis of RP is still not well understood. Recent studies have shown that ferroptosis is closely related to the death or degeneration of photoreceptor cells [23–25]. As a new form of regulated cell death, ferroptosis is characterized by lethal lipid peroxidation induced by iron-dependent accumulation of reactive oxygen species (ROS) in the cell [26]. As one of the main players in the cellular antioxidant response, nuclear factor erythroid 2-related factor 2 (NRF2), a transcriptional regulator of genes, can maintain the balance between redox and metabolism in cells [27]. It has been proven that NRF2 regulates the expression of its downstream target genes to interfere with the progression of ferroptosis and protect retinal cells [28]. As a downstream target gene of NRF2, solute carrier family 7 member 11 (SLC7A11) is considered a transmembrane protein and a principal component of the cystine/glutamate antiporter system (system xc-) that promotes the synthesis of glutathione (GSH) by mediating cystine uptake and glutamate release [29]. Glutathione synthase (GSS) catalyzes GSH synthesis, thereby affecting the activity of glutathione peroxidase 4 (GPX4) [30]. GPX4 metabolizes lipid hydroperoxides to lipid alcohols by reducing GSH levels, which influences the ROS levels and mitigates the effects of ferroptosis [31]. Yuan et al. [32] demonstrated that ferroptosis is inhibited by kaempferol, partly by activating the NRF2/SLC7A11/GPX4 signaling pathway and preventing oxygen-glucose deprivation/reperfusion-induced cell injury, confirming the potential of the NRF2/GPX4 signaling pathway to inhibit ferroptosis.

In this study, we evaluated the retinal protective effect of QST in an RP mouse model; measured the contents of iron, malondialdehyde (MDA), superoxide dismutase (SOD), and GSH in the retina; and investigated its potential mechanism by analyzing the expression of important proteins in the NRF2/GPX4 signaling pathway.

2. Material and methods

2.1. Reagents and chemicals

Huile LeDing soft capsules (Lot. GD00016262) were acquired from Guangzhou Fanle Pharmaceutical Technology Co., Ltd. (Guangzhou, China). Tropicamide-phenylephrine eye drops (Lot. MP2228) were purchased from Shentian Pharmaceutical Co., Ltd. (Jiangsu, China). Medical sodium hyaluronate gels (Lot. 190555F01) were obtained from Shanghai Qisheng Biological Preparation Co., Ltd. (Shanghai, China). Absolute ethanol (Lot. 100,092,683), xylene (Lot. 10,023,418), and neutral balsams (Lot. 10,004,160) were purchased from Sinopharm Chemical Reagent Co., Ltd. (Shanghai, China). Phosphate-buffered saline (PBS) (Lot. 01D220513) was obtained from Abiowell Biotechnology Co., Ltd. (Changsha, China). A SOD activity assay kit (Lot. 20,220,902), a reduced GSH assay kit (Lot. 20,220,907), an MDA assay kit (Lot. 20,220,727), and a tissue iron content assay kit (Lot. 20,220,627) were acquired from Beijing Solarbio Science and Technology Co., Ltd. (Beijing, China). A 4 % paraformaldehyde fixation solution (Lot. CR2201096), FAS eyeball-fixed liquid (Lot. CR2112062), eosin (Lot. CR2202010), DAPI solution (Lot. CR2201006), an anti-fluorescence quencher

(Lot. CR2202016), hematoxylin solution (Lot. CR2112051), anti-NRF2 rabbit pAb (Lot. AC220914066), an anti-GPX4 rabbit pAb (Lot. AC220914052), and Alexa Fluor 488-conjugated goat anti-rabbit IgG (Lot. CR2206040) were obtained from Wuhan Servicebio Technology Co., Ltd. (Wuhan, China). GSS antibody (Lot. 20,220,913) was purchased from Hunan Aifang Biotechnology Co., Ltd. (Hunan, China). The SLC7A11/xCT polyclonal antibody (Lot. 00115,587) was obtained from Wuhan Sanying Biology Technology Co., Ltd. (Wuhan, China).

2.2. Preparation of QST

A combination of Chinese herbs was used in QST, including GQZ (Lot. 2,201,022) and DS (Lot. 2,108,003), which were obtained from Hengxiutang Pharmaceutical Co., Ltd. (Changsha, China). Both herbs were chosen according to the Pharmacopoeia of the People's Republic of China (2015) [33], and identified by Prof. Zhi Wang from Hunan University of Chinese Medicine. The authenticated voucher specimens were preserved at the Institute of Diagnostic Research of Chinese Medicine, Hunan University of Chinese Medicine. This study used a TCM decoction method to prepare water extract of QST [34–36]. After mixing the components in a ratio of 1: 1, they were soaked for half an hour in eight times the volume of pure water, boiled for 1 h, and then filtered through a piece of gauze. The residue was boiled and filtered eight times with pure water for 1 h. Afterwards, the two filtrates were combined and concentrated to two extracts (0.26 g/ml and 0.52 g/ml QST solution) using a rotary evaporator, followed by storage at 4 °C after repackaging. Simultaneous identification of the active chemical components and quality control of QST were accomplished using a sensitive and effective ultra-performance liquid chromatography (UPLC) method (see Supplementary Material).

2.3. Animals

Forty-eight (20 male and 20 female) rd10 mice, approximately 4 weeks of age and weighing 18 ± 2 g, and 12 $C^5$7BL/6 J mice (six male and six female), approximately 4 weeks of age and weighing 18 ± 2 g, were used in this study. All mice were housed in the Laboratory Animal Center of Hunan University of Chinese Medicine under a 12-h light/dark cycle. The animals were maintained at a constant temperature of 22 °C ± 2 °C and a relative humidity of 65–75 %. All experimental protocols, including the mouse care and facility use, were conducted according to the guidelines of the Declaration of Helsinki and were authorized by the Ethics Committee of Hunan University of Chinese Medicine. The ethical batch number is LL2022042601.

2.4. Grouping and drug administration

Forty-eight rd10 mice were randomly divided into four groups: the model group (n = 12, model), positive control group (n = 12, LeDing), low-dose QST group (n = 12, QST-L), and high-dose QST group (n = 12, QST-H). The normal group was composed of 12 $C^5$7BL/6 J mice. After 1 week of acclimatization, all mice were gavaged once daily for 28 days. Mice in the normal and model groups were administered pure water orally. The positive control group received LeDing solution dissolved in peanut oil at a dosage of 0.15 g/kg/day [22]. The low and high-dose groups were administered QST orally. The recommended doses of herbal medicines for QST in TCM clinical practice are GQZ 10 g and DS 10 g, which means that the daily dose of QST for adults is 20 g [37]. The QST dose for mice was calculated according to the animal dose conversion table and body surface area [38]. The formula is as follows: the daily dosage for mice (mg/kg) = the dose of crude drug for adults (20 g) ÷ the average human body weight (70 kg) × W (W = 9.1) [39]. For example, the calculation of 20 g divided by 70 kg multiplied by 9.1 results in a dosage of 2.6 g/kg. The low-dose group was administered this dose, whereas the high-dose group received twice as much, equivalent to 5.2 g/kg.

2.5. Histopathological examination of retinal tissue

Fresh eyeball samples from each group were preserved in a 4 % paraformaldehyde-fixed solution for 24 h, dehydrated, embedded in paraffin, and sectioning (approximately 4 μm). Next, the sections were dewaxed in xylene, dehydrated with gradient ethanol, and sequentially stained with hematoxylin and eosin (H&E) staining. The structural characteristics of the samples were examined using a light microscope (Nikon Eclipse; Nikon, Japan). Image J (NIH, Bethesda, MD, USA) software was used to determine the thickness and number of outer nuclear layers (ONLs).

2.6. Measurement of retinal function by scotopic electroretinography (ERG) analysis

The mice were subjected to a 12-h dark adaptation period before scotopic ERG analysis. Using a light-proof box, the mice were transferred from the dark room to the experimental room and subsequent experiments were conducted under dim red light. Mice were deeply anesthetized using abdominal injection of 1 % sodium pentobarbital (60 mg/kg). All mice were treated with tropicamide phenylephrine eye drops to dilate both eyes and sodium hyaluronate eye gel to keep the eyes moist. After fixing the animals, eye electrodes were placed on the contact lenses, the ground electrode was placed under the animal's tail, and the reference electrode was placed under the animal's forehead. A relatively stable waveform was obtained before images were captured with the mouse cornea in contact with the imaging microscope (Micron IV; Phoenix Research Laboratories, Inc., Pleasanton, CA, USA).

2.7. Imaging and measurement of the morphological structure of fundus blood vessels

After sufficient anesthesia and administration of mydriasis, the mice were placed on the operating table to perform subsequent procedures. The images were captured using a retinal imaging microscope (Micron IV; Phoenix Research Laboratories Inc.). To capture the bright-field images using Micron IV, the exciter and barrier filters were set to 1. The body position and distance from the eyeball were adjusted to obtain a clear central field of vision of the pupil. The spiral ring of the microscope was moved until a retinal image was presented. The light source intensity and focus buttons were used to adjust the image until it became clear; then, a snapbutton was clicked to capture it.

2.8. Continuous measurement of retinal blood flow

Following anesthesia, the animals were placed in a stereotaxic holder fixed beneath an RFLSI Pro instrument (RWD Life Technology Co., Ltd., Shenzhen, China). The retina was illuminated with a 784-nm, 32-mW laser at a 30° angle, and the intensity of the measuring light was adjustable. Using a CCD camera and a time exposure of 10 m s per frame over 300 frames, an image acquisition system captured the blood flow. To calculate the mean blood flow index of the retinal tissue, a region of interest (ROI) was selected at the location where the laser targeted the retina [40].

2.9. Measurement of the iron level in retinal tissues

The homogenate was centrifuged and the supernatant was collected after sample extraction. The iron content of the retinal tissue was determined using a tissue iron content assay kit according to the manufacturer's instructions.

2.10. Assessment of MDA, SOD, and GSH levels in retinal tissues

After sample extraction, the homogenate was centrifuged to collect the supernatant. Based on the manufacturer's instructions, the levels of MDA, SOD, and GSH in the supernatant were determined using the appropriate ELISA kit.

2.11. Molecular docking between the drug candidate and their targets

Silicoprotein ligand docking software AutoDock Vina 1.2.2 (https://vina.scripps.edu/) was used to determine the binding affinity between the candidate drug and its target and explore the interaction mode. The molecular structures of rutin and tanshinone IIA were obtained from PubChem (https://pubchem.ncbi.nlm.nih.gov/). The 3D structures of NRF2, SLC7A11, GSS, and GPX4 protein receptors were obtained from the RCSB Protein Data Bank database (https://www.rcsb.org/). The entry IDs used were 3ZGC, 7P9U, 2HGS, and 6HN3, respectively. Before docking, the complex ligand and water molecules were stripped from the crystal structure. Each protein and molecular file was converted into PDBQT format after hydrogen atoms were added to all proteins and ligands. In AutoDock Vina, ligands and receptors were connected, and model visualization was performed. Based on the optimal docking fraction, the most likely binding conformation of the ligand in the active sites was selected based on the free binding energy (kcal/mol).

2.12. Immunofluorescence staining for NRF2, SLC7A11, GSS, and GPX4 in retinal tissues

The paraffin sections were deparaffinized using xylene and alcohol, followed by antigen repair. Next, 5 % BSA in PBS was used to block the slices for 30 min after addition of the autofluorescence quenching agent. All primary antibodies were diluted 1: 1000 and incubated at 4 °C overnight. A PBS rinse was performed three times for 5 min on each section. Following that, sections were incubated for 50 min at room temperature in the dark with Alexa Fluor 488-conjugated goat anti-rabbit IgG conjugated at 1: 200. To stain the nuclei of the specimens, they were rinsed three times with PBS for 5 min each time, followed by the dropwise addition of DAPI and incubation at room temperature in the dark for 10 min. A fluorescence microscope (Nikon) was used to collect images after washing off the excess DAPI from the sections and sealing them with an anti-fluorescence quencher. Fluorescence intensity analysis was performed on each captured image using Image-Pro Plus 6.0 (Rockville, MD, USA).

2.13. Statistical analysis

Statistical analysis was conducted using Statistical Package for Social Sciences (SPSS) version 26.0 (IBM Corp., Armonk, NY, USA). All experiments were repeated at least three times. Values are expressed as the average ± standard deviation (SD). To determine the significance of the differences between groups, one-way analysis of variance (ANOVA) was used, followed by Dunnett's multiple comparisons. $P < 0.05$ was considered statistically significant.

3. Results

3.1. Histopathological evaluation of retinal tissue

H&E staining was performed on the retinal tissues of each group to observe the effects of QST on the overall morphology of the

retina. As shown in Fig. 1A, the structure of retinal tissues in the normal group was clear. In the retina, the cells were morphologically and structurally normal, with evenly stained inner nuclear layers (INLs) and ONLs that were delineated and clearly demarcated. Compared with the normal group, the retinal structure of the model group exhibited thinning of the retina, with an unclear boundary between the INLs and ONLs and obvious atrophy or complete disappearance of the ONL. However, after 28 days of intragastric treatment, there was good retinal protection in all three drug treatment groups compared with the model group, as demonstrated by the following factors, the thickness of the retina increased, the boundary between the INLs and ONLs reappeared, and ONL atrophy improved significantly. As shown in Fig. 1B and C, the thickness and number of ONLs in the model group were significantly lower than those in the normal group ($P < 0.01$). In comparison with the model group, the thickness and number of ONLs in the QST low-dose and high-dose groups were significantly increased ($P < 0.01$).

3.2. Effect of QST on retinal function

We performed ERG measurements to study the physiological consequences of the changes observed in retinal histology and investigated the influence of QST on retinal function. The recorded ERG waveforms are shown in Fig. 2A, and the quantification of the mean maximum amplitudes of the a and b-waves are shown in Fig. 2B and C, respectively. Both amplitudes were significantly lower in the model group than in the normal group ($P < 0.01$). Compared with the model group, the average amplitudes of the a-waves of the QST low and high-dose groups increased by 106.8 % and 334.8 %, respectively. Additionally, comparison with the model group showed that the average amplitudes of the b-waves in the QST low-dose and high-dose groups increased by 101.9 % and 364.8 %, respectively.

3.3. Effect of QST on fundus structure and vascular morphology

Fundus photography was used to observe changes in the fundus visual field and vascular structure of the mice in each group. According to the fundus examination in the normal group (Fig. 3A), the optic discs were healthy, the retinal vascular architecture was intact, and the background of the fundus was clear. However, there was poor visibility of the fundus in the model group (Fig. 3B) owing to large pigmentation, atrophy of the optic disc, and blurring of the main retinal vascular structures. A certain extent of improvement was observed in the fundus condition of the positive control, low-dose QST, and high-dose QST groups after drug treatment. Fig. 3C–E shows that the vascular structures of the positive control, QST low-dose, and QST high-dose groups were much clearer than those of the model group.

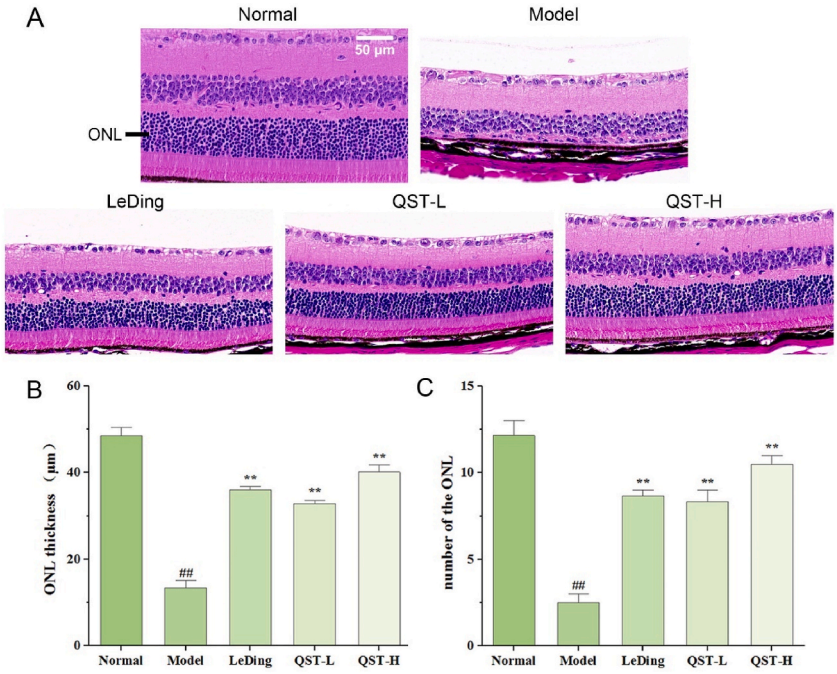

Fig. 1. Effect of QST on pathological manifestations in retinal tissues in the mouse model of RP. A. The representative histological photos of retinal sections stained with H&E (400 ×). B. The morphological analysis on the thickness of the ONL in retinal tissues in five experimental groups of mice. C. The morphological analysis on the number of the ONL in retinal tissues in five experimental groups of mice. Data are expressed as mean ± SD (n = 6). $^{\#\#}P < 0.01$, compared with the normal group; $^{**}P < 0.01$, compared with the model group.

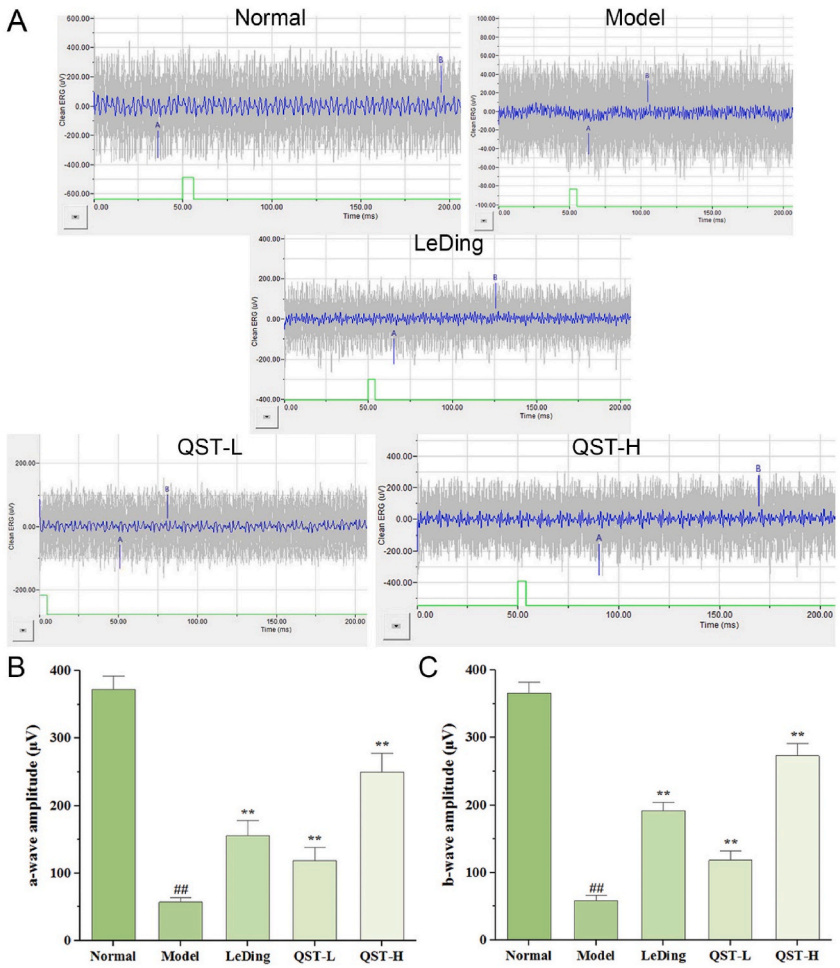

Fig. 2. Effect of QST on the changes of retinal tissue function. A. The waveform results of ERG detection in five groups of mice. B. The average amplitudes of the a-waves in five groups. C. The average amplitudes of the b-waves in five groups. Results are expressed as mean ± SD (n = 6). $^{\#\#}P < 0.01$, compared with the normal group; $^{**}P < 0.01$, compared with the model group.

3.4. Effect of QST on retinal blood flow

To further verify the effects of QST on retinal tissue vascular function and microcirculation, real-time monitoring of blood flow perfusion in living retinal tissue was performed using a laser speckle contrast imaging (LSCI) system. There was a significant difference in retinal microcirculation blood flow between rd10 and normal mice. As shown in Fig. 4A and B, blood flow in the retinal tissue expressed as integrated optic density (IOD) was significantly lower in the model group than in the normal group ($P < 0.01$). However, it is important to note that QST can make a significant difference in this situation. Compared with the model group, the QST low-dose and high-dose groups showed increased retinal blood flow of 28 % and 84 %, respectively.

3.5. Effect of QST on iron level

Healthy intracellular iron homeostasis is essential for retinal metabolism and phototransduction because excessive iron accumulation in the body can damage retinal cells. Fig. 5 shows the effect of QST on iron levels in the retinal tissue. Compared with the normal group, the level of iron in the retina of the model group was significantly higher ($P < 0.01$). In contrast, the QST low-dose and high-dose groups showed decreased retinal iron levels of 22.7 % and 55.1 %, respectively, compared with the model group.

3.6. Effect of QST on the levels of oxidative stress markers

As shown in Fig. 6A, the level of MDA was significantly higher in the model group than in the normal group ($P < 0.01$), whereas the level of MDA was markedly reduced in the QST low-dose and high-dose groups compared with the model group ($P < 0.01$). The SOD and GSH levels (Fig. 6B and C) were markedly reduced in the model group compared with the normal group ($P < 0.01$), while the two

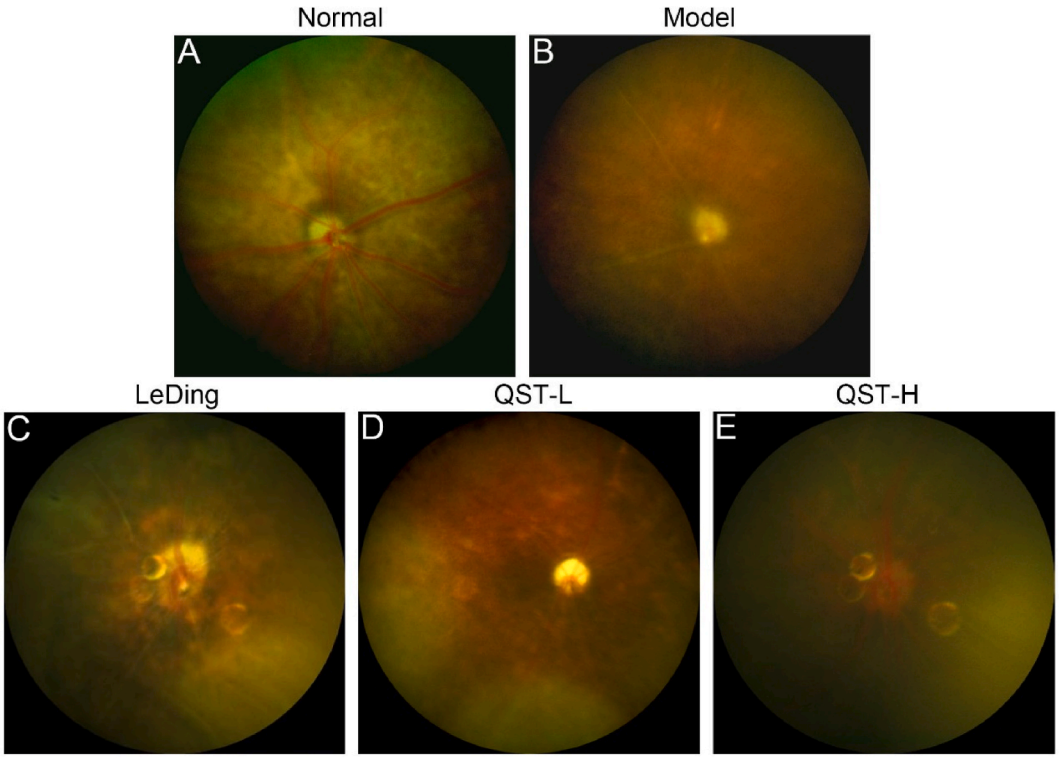

Fig. 3. QST treatment improves fundus structure and vascular morphology. The results of fundus photography in the normal (A), model (B), LeDing (C), QST-L (D), and QST-H (E) groups.

levels were significantly increased in the QST low-dose and high-dose groups compared with the model group ($P < 0.01$).

3.7. Results of molecular docking between active ingredients of QST and the NRF2/GPX4 signaling pathway

According to the UPLC results, rutin and tanshinone IIA were the effective chemical constituents of QST. To investigate whether QST molecules bind well to NRF2/GPX4 signaling pathway targets at the atom level, we performed molecular docking analysis. As shown in Fig. 7A and B, we obtained the binding postures and interaction models of two small ligand molecules with four target proteins and recorded the binding energies generated by each interaction in Table 1. According to the results, the small molecules of both ligands bound to the target protein through visible hydrogen bonds. These small molecules showed strong binding activity and high stability for NRF2 and SLC7A11, relative binding activity for GPX4, and certain binding activity for GSS.

3.8. Effect of QST on the expression and localization of NRF2, SLC7A11, GSS, and GPX4 proteins in the retinal tissue

As shown in Fig. 8**A-C**, the protein expression levels of NRF2 and SLC7A11 in the model group were significantly lower than those in the normal group ($P < 0.01$). A comparison of the low-dose QST group with the model group revealed that NRF2 and SLC7A11 protein levels increased significantly by 179.1 % and 83.7 %, respectively. In addition, compared with the model group, the protein levels of NRF2 and SLC7A11 in the high-dose group increased by 261.7 % and 127.9 % respectively. As shown in Fig. 9**A-C**, the expression levels of GSS and GPX4 in the model group were significantly lower than those in the normal group ($P < 0.01$). In our study, the low-dose QST group showed 172 % and 364.4 % higher expression of GSS and GPX4, respectively, than the model group. Compared with the model group, the high-dose QST group exhibited 302 % and 483.2 % higher expressions of GSS and GPX4 proteins, respectively.

4. Discussion

RP is a hereditary fundus disease characterized by the death of a large number of rod cells and degeneration of cone cells due to gene mutations, resulting in vision impairment or blindness [41]. As a supplement for treating patients with RP, GQZ can delay the progression of visual cone degeneration by providing neuroprotective effects [18]. By regulating the expression of STAT3 and CCL2 and activating the MAPK signaling pathway, zeaxanthin dipalmitate in the GQZ may delay photoreceptor degeneration and protect the retina in rd10 mice [42]. *Lycium barbarum* polysaccharides possibly protect photoreceptor cells from photo-induced retinal damage by upregulating NRF2 and TRXR1 [43].

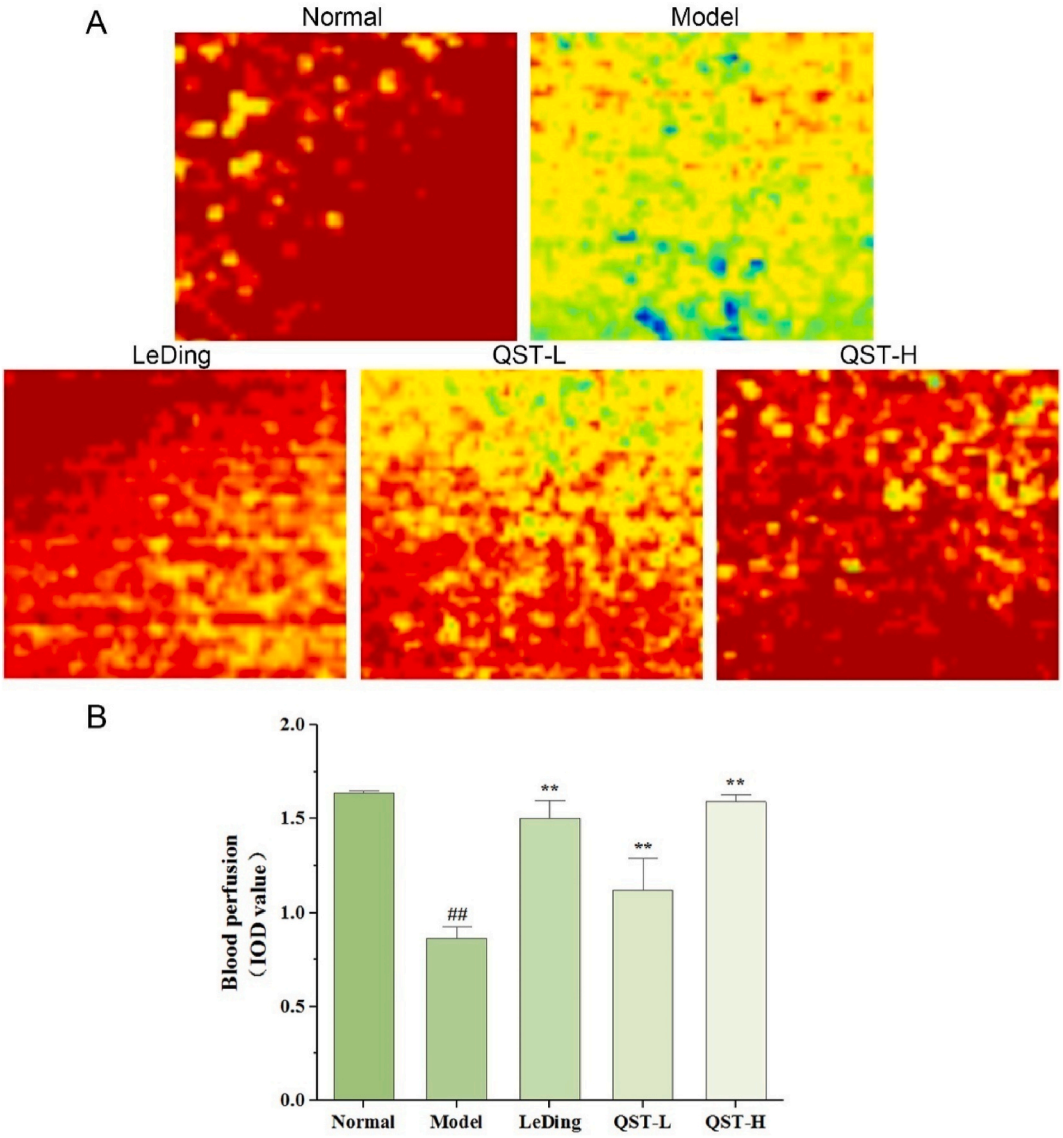

Fig. 4. QST treatment improves retinal blood perfusion. A. The representative images of regional blood flow in the retinal tissues of mice in five groups. Blue indicates low blood flow, yellow or green represents intermediate blood flow, and red denotes high blood flow. B. Measurement of the blood flow in the retinal tissues using a quantitative method. Values are expressed as mean ± SD (n = 6). $^{\#\#}P < 0.01$, compared with the normal group; $^{**}P < 0.01$, compared with the model group.

Retinal vascular stenosis is a change in the visual field of the fundus in patients with RP [4]. Researchers have shown that retinal vascular stenosis affects the extent of visual field defects in patients with RP [44]. Modern pharmacological research has confirmed that tanshinone, the active ingredient of DS, exhibits antiplatelet aggregation, dilation of blood vessels, increases blood flow, and improves microcirculation [45].

This study focused on the protective effects of QST on mouse model of RP. H&E staining results showed that after treatment with QST, the structure of each layer of the retina of rd10 mice was relatively regular, and the number of layers of photoreceptors in the ONL of the retina and the density of the nuclei were improved compared with those in the model group, indicating that QST could enable the retina of rd10 mice to retain more photoreceptors, which had a certain protective effect on the retinal tissue. ERG is a non-invasive method for evaluating retinal function that can help diagnose RP and determine the extent of damage to the visual system. The a-wave represents the potential change in photoreceptor cells, whereas the b-wave represents the potential change in conduction neurons [46]. From the amplitude changes of the a and b-waves, it was observed that QST could protect the photoreceptors to some extent to retain some visual functions. These results indicated that QST is a potential complementary therapy for RP.

Several studies have demonstrated that structural changes in the vascular system and microvascular dysfunction contribute significantly to RP [47]. We performed fundus photographic detection to facilitate a more intuitive judgment of fundus status. The

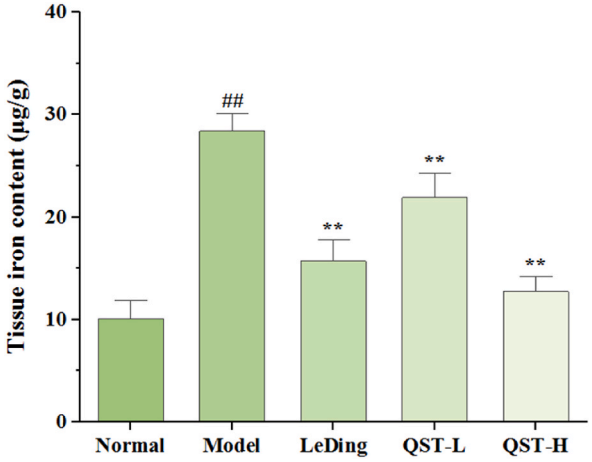

Fig. 5. Effect of QST on retinal tissues iron contents measured in the mouse model of RP. Data are expressed as mean ± SD (n = 6). $^{\#\#}P < 0.01$, compared with the normal group; $^{**}P < 0.01$, compared with the model group.

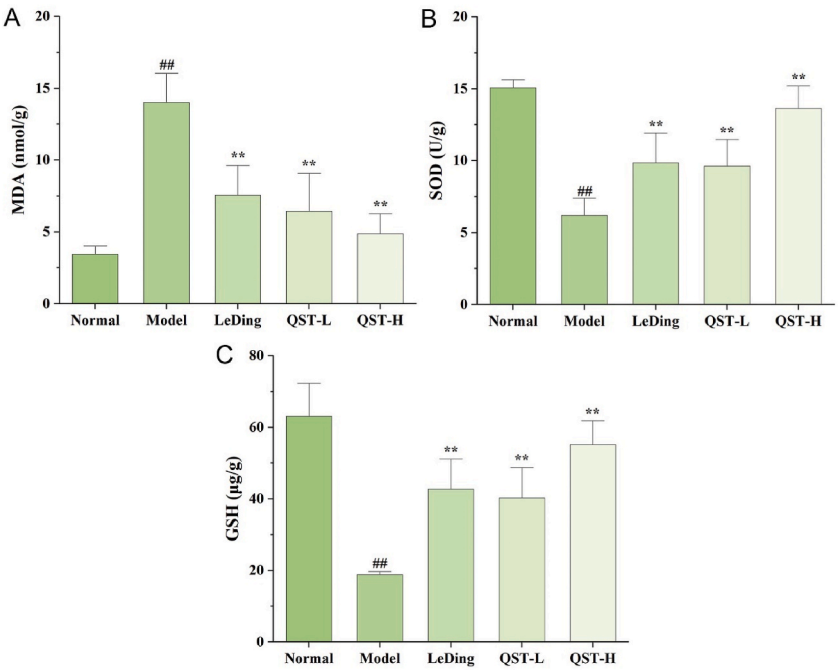

Fig. 6. Effect of QST on the levels of MDA (A), SOD (B), and GSH (C) in the mouse model of RP. Results are expressed as mean ± SD (n = 6). $^{\#\#}P < 0.01$, compared with the normal group; $^{**}P < 0.01$, compared with the model group.

results showed a more complete retinal vascular structure in mice treated with QST than in the model group mice. Accordingly, QST appears to improve the structure of eyeground blood vessels in retinal tissue. To compensate for the inability of fundus photography to distinguish changes in retinal microcirculation, we measured blood perfusion in mouse retinas using the LSCI system [48]. The model group showed a significant decrease in retinal blood flow perfusion volume, whereas mice treated with QST showed a significant increase in tissue irrigation volume. QST improves retinal microcirculation and increases retinal blood flow in rd10 mice.

The results of an *in vivo* experiment showed that rd10 mice experienced changes in retinal iron homeostasis during retinal degeneration, as evidenced by significant increases in the levels of retinal ferritin, ferritin bound iron, transferrin, and total iron [49]. Evidence also suggests that ferrous ions accumulate during sodium iodate-induced retinal degeneration [50]. These data support the hypothesis that iron ions accumulate in the retinas of rd10 mice. Several studies have shown that injecting ferrous ions into the vitreous bodies of mice leads to the death of photoreceptor cells, accumulation of superoxide radicals, and lipid peroxidation [51,52]. Moreover, when a sodium iodate-induced RP model was used to verify the correlation between RP and ferroptosis, the researchers found that sodium iodate reduced GSH levels and increased iron and ROS levels, leading to lipid damage and ferroptosis in RPE cells

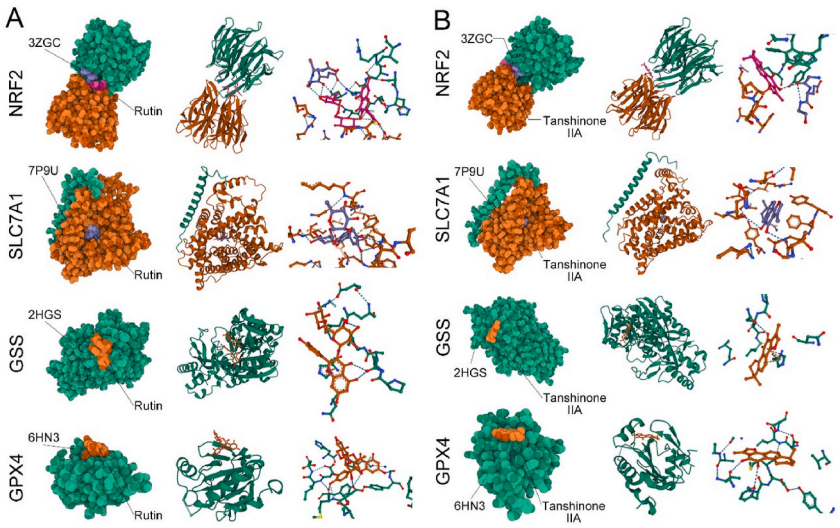

Fig. 7. Docking results of active ingredients of QST and the NRF2/GPX4 signaling pathway. A. Docking results of rutin and target proteins. B. Docking results of tanshinone IIA and target proteins. The first column is a spherical diagram of molecular docking. The second column is the docking results at the same level as the first column of images. The proteins are depicted in cartoons, ligands in ball-and-sticks. In the third column, we can see a partial magnified view of the interaction between receptors and ligands in the second column.

Table 1
Binding energy of small molecular compounds to target proteins.

Target proteins	Small molecular	Binding energy (kcal/mol)
NRF2 (3ZGC)	Rutin	−8.182
NRF2 (3ZGC)	Tanshinone IIA	−7.812
SLC7A11 (7P9U)	Rutin	−9.779
SLC7A11 (7P9U)	Tanshinone IIA	−8.39
GSS (2HGS)	Rutin	−3.685
GSS (2HGS)	Tanshinone IIA	−4.129
GPX4 (6HN3)	Rutin	−6.565
GPX4 (6HN3)	Tanshinone IIA	−6.067

[23]. These studies indicate that RP may be involved in ferroptosis. SOD and GSH have been shown to be important antioxidants in the body, which play an important role in clearing excess ROS and protecting the retinal phospholipid membrane [53,54]. Importantly, however, when the accumulation of ROS in the body exceeds the body's capacity for self-clearance, it not only causes excessive consumption of SOD and GSH, but also produces a large number of lipid peroxidation products, such as MDA [55]. Our results showed that compared with the model group, the iron and MDA levels in the retina of the QST intervention group mice were significantly reduced, while SOD and GSH levels were significantly increased. Based on these findings, we hypothesized that the mechanism of action of QST in RP is related to ferroptosis.

A growing number of studies have shown that NRF2/GPX4 signaling plays a key role in regulating ferroptosis [56,57]. As an enzyme involved in protecting the lipid bilayer of the cell membrane, GPX4 inhibits the formation and accumulation of lipid ROS [58]. GPX4 protein levels in cells are thought to influence the sensitivity to ferroptosis. Disruption of the redox balance between cells occurs when the GPX4 protein is inactivated, thus causing ferroptosis [58]. As an important co-factor of the GPX4 catalytic peroxide, GSH synthesis is affected by cysteine concentration, which is regulated by the system xc- [55]. Simultaneously, GSS plays a crucial role in this process. NRF2 is an important transcription factor that inhibits ferroptosis by regulating the transcription of SLC7A11 [32]. Our immunofluorescence results that GPX4, GSS, SLC7A11, and NRF2 were significantly reduced in the model group. Conversely, QST significantly increased the expression of NRF2 protein in the retinal tissue and activated the downstream antioxidant target gene SLC7A11 by enhancing its ability to function, and promoting the synthesis of GSS to improve the activity of GPX4. According to these findings, QST may alleviate RP by inhibiting ferroptosis via regulation of the NRF2/GPX4 signaling pathway.

5. Conclusions

This study showed that treatment of rd10 mice with QST delayed the progression of RP. Improved shape and function of the retinal tissue, as well as increased blood flow to the tissue, account for the protective effects of QST on the retinal tissue. Because of its ability to decrease the content of iron and MDA and increase the concentrations of SOD and GSH, QST plays a role in partial antioxidation and the prevention of ferroptosis. Furthermore, this study provides the first evidence that QST protects retinal tissue against ferroptosis by

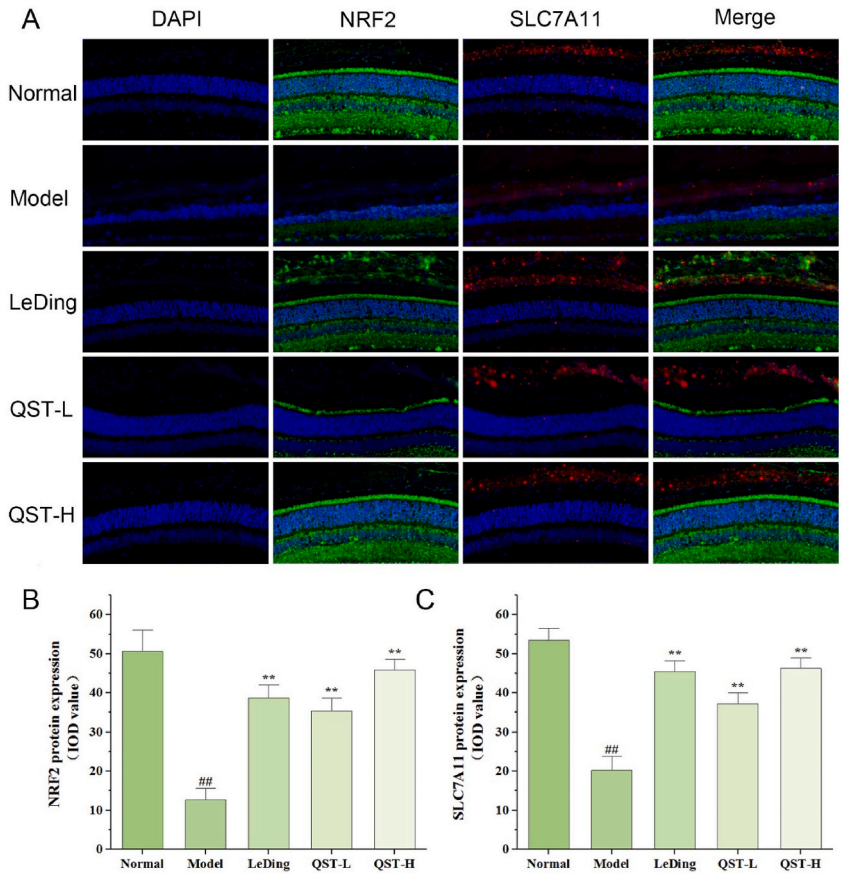

Fig. 8. The expression of NRF2 and SLC7A11 proteins increased in retinal tissues of RP model mouse following QST treatment. A. Immunofluorescence staining results of retinal tissues in different groups. The sections were counterstained with DAPI (blue) in order to visualize the expression and localization of NRF2 (green) and SLC7A11 (red). Magnification, 400 × . B. Quantitative fluorescence analysis of NRF2 protein in the retina. C. Quantitative fluorescence analysis of SLC7A11 protein in the retina. Values are expressed as mean ± SD (n = 6). $^{\#\#}P < 0.01$, compared with the normal group; $^{**}P < 0.01$, compared with the model group.

activating the NRF2/GPX4 signaling pathway.

Funding

This study was supported by the National Natural Science Foundation of China (nos. 82,004,427 and 82,374,429), Natural Science Foundation of Hunan Province (nos. 2023JJ30460 and 2023JJ40474), Science and Technology Innovation Program of Hunan Province (no. 2021RC3101), China Postdoctoral Science Foundation (no. 2019M662790), Key Project of Science Research of Hunan Provincial Education Department (no. 21A0240), and Guidance Project of Academician Liu Liang's Expert Workstation (no. 22YS003).

Data availability statement

Data included in article/supplementary material/referenced in article.
Supplementary content related to this article has been published online at [URL].

Ethics statement

This study was reviewed and approved by the Ethics Committee of Hunan University of Chinese Medicine, with the approval number: LL2022042601.

CRediT authorship contribution statement

Meng Xiong: Writing – original draft, Methodology, Data curation, Conceptualization. **Chen Ou:** Methodology, Data curation. **Chang Yu:** Methodology. **Jingyue Qiu:** Methodology. **Jing Lu:** Data curation. **Chaojun Fu:** Data curation. **Qinghua Peng:**

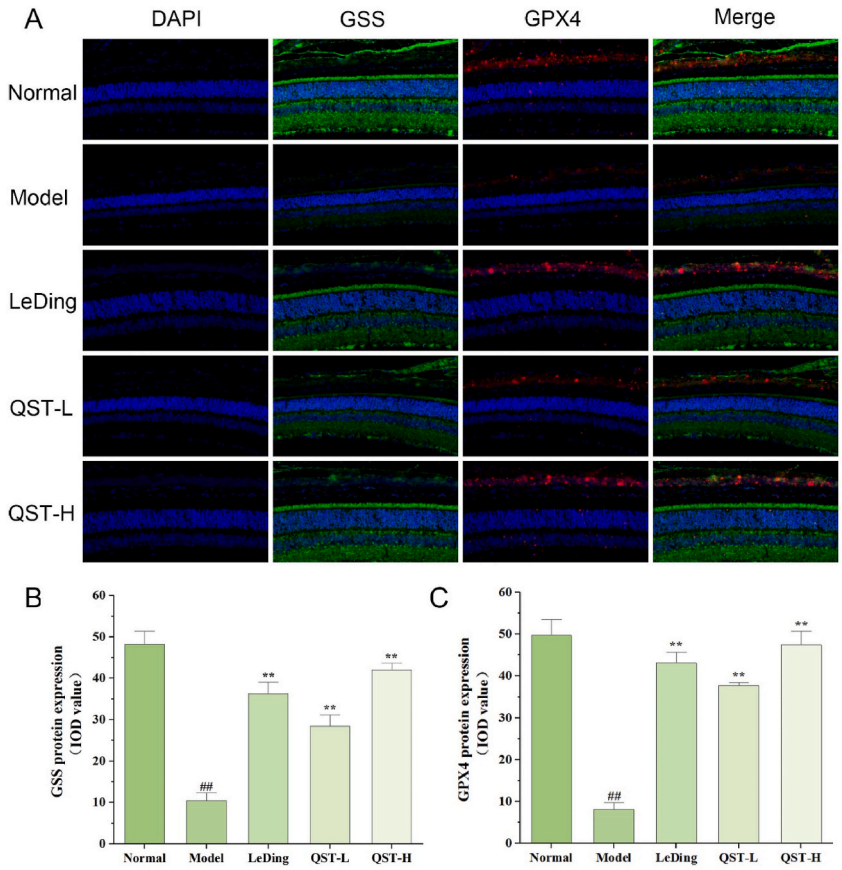

Fig. 9. The expression of GSS and GPX4 proteins increased in retinal tissues of RP model mouse following QST treatment. A. Immunofluorescence staining results of retinal tissues in different groups. The sections are counterstained with DAPI (blue) in order to visualize the expression and localization of GSS (green) and GPX4 (red). Magnification, 400 × . B. Quantitative fluorescence analysis of GSS protein in the retina. C. Quantitative fluorescence analysis of GPX4 protein in the retina. Results are expressed as mean ± SD (n = 6). $^{\#\#}P < 0.01$, compared with the normal group; $^{**}P < 0.01$, compared with the model group.

Conceptualization. **Meiyan Zeng:** Writing – review & editing, Funding acquisition, Conceptualization. **Houpan Song:** Writing – review & editing, Funding acquisition, Conceptualization.

Declaration of competing interest

The authors declare that they have no known competing financial interests or personal relationships that could have appeared to influence the work reported in this paper.

Appendix A. Supplementary data

Supplementary data to this article can be found online at https://doi.org/10.1016/j.heliyon.2023.e22443.

References

[1] V. Busskamp, J. Duebel, D. Balya, M. Fradot, T.J. Viney, S. Siegert, A.C. Groner, E. Cabuy, V. Forster, M. Seeliger, M. Biel, P. Humphries, M. Paques, S. Mohand-Said, D. Trono, K. Deisseroth, J.A. Sahel, S. Picaud, B. Roska, Genetic reactivation of cone photoreceptors restores visual responses in retinitis pigmentosa, Science 329 (2010) 413–417, https://doi.org/10.1126/science.1190897.
[2] D.T. Hartong, E.L. Berson, T.P. Dryja, Retinitis pigmentosa, Lancet 368 (2006) 1795–1809, https://doi.org/10.1016/S0140-6736(06)69740-7.
[3] S.K. Verbakel, R.A.C. van Huet, C.J.F. Boon, A.I. den Hollander, R.W.J. Collin, C.C.W. Klaver, C.B. Hoyng, R. Roepman, B.J. Klevering, Non-syndromic retinitis pigmentosa, Prog. Retin. Eye Res. 66 (2018) 157–186, https://doi.org/10.1016/j.preteyeres.2018.03.005.
[4] S.G. Schwartz, X. Wang, P. Chavis, A.E. Kuriyan, S.A. Abariga, Vitamin A and fish oils for preventing the progression of retinitis pigmentosa, Cochrane Database Syst. Rev. 6 (2020) CD008428, https://doi.org/10.1002/14651858.CD008428.pub3.

[5] D. Dalkara, K.D. Kolstad, K.I. Guerin, N.V. Hoffmann, M. Visel, R.R. Klimczak, D.V. Schaffer, J.G. Flannery, AAV mediated GDNF secretion from retinal glia slows down retinal degeneration in a rat model of retinitis pigmentosa, Mol. Ther. 19 (2011) 1602–1608, https://doi.org/10.1038/mt.2011.62.

[6] D. Meng, S.D. Ragi, S.H. Tsang, Therapy in rhodopsin-mediated autosomal dominant retinitis pigmentosa, Mol. Ther. 28 (2020) 2139–2149, https://doi.org/10.1016/j.ymthe.2020.08.012.

[7] M. Zarbin, Cell-based therapy for degenerative retinal disease, Trends Mol. Med. 22 (2016) 115–134, https://doi.org/10.1016/j.molmed.2015.12.007.

[8] M.F. Dias, K. Joo, J.A. Kemp, S.L. Fialho, A. da Silva Cunha, S.J. Woo, Y.J. Kwon, Molecular genetics and emerging therapies for retinitis pigmentosa: basic research and clinical perspectives, Prog. Retin. Eye Res. 63 (2018) 107–131, https://doi.org/10.1016/j.preteyeres.2017.10.004.

[9] A. Zheng, Y. Li, S.H. Tsang, Personalized therapeutic strategies for patients with retinitis pigmentosa, Expet Opin. Biol. Ther. 15 (2015) 391–402, https://doi.org/10.1517/14712598.2015.1006192.

[10] Y.M. Lee, Y.-R. Lee, C.-S. Kim, K. Jo, E. Sohn, J.S. Kim, J. Kim, Effect of guibi-tang, a traditional herbal formula, on retinal neovascularization in a mouse model of proliferative retinopathy, Int. J. Mol. Sci. 16 (2015) 29900–29910, https://doi.org/10.3390/ijms161226211.

[11] Y. Tang, B. Zhu, J. Shi, Q. Liu, L. Chen, Q. Peng, J. Peng, X. Yao, Effects of Qingguang'an Granules on mitochondrial autophagy of retinal ganglion cells in rats with chronic ocular hypertension, Digital Chinese Medicine 5 (2022) 295–304.

[12] H. Ai, F. Xia, B. Li, X. Chen, J. Peng, Q. Peng, Comprehensive treatment of retinitis pigmentosa in traditional Chinese medicine and analysis of medication rules, J. Hunan Univ. Chinese Med. 40 (2020) 165–169.

[13] X. Li, P. Jiang, H. Ai, J. Peng, Q. Peng, Discussion on the rule of Chinese medicine treatment of retinitis pigmentosa based on cluster Analysis, J. Hunan Univ. Chinese Med. 40 (2020) 792–796.

[14] K. Neelam, S. Dey, R. Sim, J. Lee, K.-G. Au Eong, Fructus lycii: a natural dietary supplement for amelioration of retinal diseases, Nutrients 13 (2021) 246, https://doi.org/10.3390/nu13010246.

[15] F.-C. Hsieh, C.-T. Hung, K.-C. Cheng, C.-Y. Wu, Y.-C. Chen, Y.-J. Wu, W. Liu, C.-C. Chiu, Protective effects of Lycium barbarum extracts on UVB-induced damage in human retinal pigment epithelial cells accompanied by attenuating ROS and DNA damage, Oxid. Med. Cell. Longev. 2018 (2018), 4814928, https://doi.org/10.1155/2018/4814928.

[16] F. Liu, J. Zhang, Z. Xiang, D. Xu, K.-F. So, N. Vardi, Y. Xu, Lycium barbarum polysaccharides protect retina in rd1 mice during photoreceptor degeneration, Invest. Ophthalmol. Vis. Sci. 59 (2018) 597–611, https://doi.org/10.1167/iovs.17-22881.

[17] K. Wang, J. Xiao, B. Peng, F. Xing, K.-F. So, G.L. Tipoe, B. Lin, Retinal structure and function preservation by polysaccharides of wolfberry in a mouse model of retinal degeneration, Sci. Rep. 4 (2014) 7601, https://doi.org/10.1038/srep07601.

[18] H.H.-L. Chan, H.-I. Lam, K.-Y. Choi, S.Z.-C. Li, Y. Lakshmanan, W.-Y. Yu, R.C.-C. Chang, J.S.-M. Lai, K.-F. So, Delay of cone degeneration in retinitis pigmentosa using a 12-month treatment with Lycium barbarum supplement, J. Ethnopharmacol. 236 (2019) 336–344, https://doi.org/10.1016/j.jep.2019.03.023.

[19] H. Zhang, Y. Liu, Q. Jiang, K. Li, Y. Zhao, C. Cao, J. Yao, Salvianolic acid A protects RPE cells against oxidative stress through activation of Nrf2/HO-1 signaling, Free Radic. Biol. Med. 69 (2014) 219–228, https://doi.org/10.1016/j.freeradbiomed.2014.01.025.

[20] X. Liu, C. Xavier, J. Jann, H. Wu, Salvianolic acid B (sal B) protects retinal pigment epithelial cells from oxidative stress-induced cell death by activating glutaredoxin 1 (Grx1), Int. J. Mol. Sci. 17 (2016) E1835, https://doi.org/10.3390/ijms17111835.

[21] C. Ou, W. Xie, P. Jiang, Y. Wang, J. Peng, Y. Zhou, H. Song, Q. Peng, Lycium barbarum L. and Salvia miltiorrhiza Bunge protect retinal pigment epithelial cells through endoplasmic reticulum stress, J. Ethnopharmacol. 296 (2022), 115519, https://doi.org/10.1016/j.jep.2022.115519.

[22] C. Ou, P. Jiang, Y. Tian, Z. Yao, Y. Yang, J. Peng, M. Zeng, H. Song, Q. Peng, Fructus Lycii and Salvia miltiorrhiza Bunge extract alleviate retinitis pigmentosa through Nrf2/HO-1 signaling pathway, J. Ethnopharmacol. 273 (2021), 113993, https://doi.org/10.1016/j.jep.2021.113993.

[23] B. Liu, W. Wang, A. Shah, M. Yu, Y. Liu, L. He, J. Dang, L. Yang, M. Yan, Y. Ying, Z. Tang, K. Liu, Sodium iodate induces ferroptosis in human retinal pigment epithelium ARPE-19 cells, Cell Death Dis. 12 (2021) 230, https://doi.org/10.1038/s41419-021-03520-2.

[24] J.-J. Lee, G.-P. Chang-Chien, S. Lin, Y.-T. Hsiao, M.-C. Ke, A. Chen, T.-K. Lin, 5-Lipoxygenase inhibition protects retinal pigment epithelium from sodium iodate-induced ferroptosis and prevents retinal degeneration, Oxid. Med. Cell. Longev. 2022 (2022), 1792894, https://doi.org/10.1155/2022/1792894.

[25] Z. Tang, M. Huo, Y. Ju, X. Dai, N. Ni, Y. Liu, H. Gao, D. Zhang, H. Sun, X. Fan, Y. Chen, P. Gu, Nanoprotection against retinal pigment epithelium degeneration via ferroptosis inhibition, Small Methods 5 (2021), e2100848, https://doi.org/10.1002/smtd.202100848.

[26] B.R. Stockwell, J.P. Friedmann Angeli, H. Bayir, A.I. Bush, M. Conrad, S.J. Dixon, S. Fulda, S. Gascón, S.K. Hatzios, V.E. Kagan, K. Noel, X. Jiang, A. Linkermann, M.E. Murphy, M. Overholtzer, A. Oyagi, G.C. Pagnussat, J. Park, Q. Ran, C.S. Rosenfeld, K. Salnikow, D. Tang, F.M. Torti, S.V. Torti, S. Toyokuni, K.A. Woerpel, D.D. Zhang, Ferroptosis: a regulated cell death nexus linking metabolism, redox Biology, and disease, Cell 171 (2017) 273–285, https://doi.org/10.1016/j.cell.2017.09.021.

[27] A. Anandhan, M. Dodson, C.J. Schmidlin, P. Liu, D.D. Zhang, Breakdown of an ironclad defense system: the critical role of NRF2 in mediating ferroptosis, Cell Chem. Biol. 27 (2020) 436–447, https://doi.org/10.1016/j.chembiol.2020.03.011.

[28] Z. Xu, Y. Wei, J. Gong, H. Cho, J.K. Park, E.-R. Sung, H. Huang, L. Wu, C. Eberhart, J.T. Handa, Y. Du, T.S. Kern, R. Thimmulappa, A.J. Barber, S. Biswal, E. J. Duh, NRF2 plays a protective role in diabetic retinopathy in mice, Diabetologia 57 (2014) 204–213, https://doi.org/10.1007/s00125-013-3093-8.

[29] P. Koppula, L. Zhuang, B. Gan, Cystine transporter SLC7A11/xCT in cancer: ferroptosis, nutrient dependency, and cancer therapy, Protein Cell 12 (2021) 599–620, https://doi.org/10.1007/s13238-020-00789-5.

[30] Y.P. Kang, A. Mockabee-Macias, C. Jiang, A. Falzone, N. Prieto-Farigua, E. Stone, I.S. Harris, G.M. DeNicola, Non-canonical glutamate-cysteine ligase activity protects against ferroptosis, Cell Metabol. 33 (2021) 174–189.e7, https://doi.org/10.1016/j.cmet.2020.12.007.

[31] K. Bersuker, J.M. Hendricks, Z. Li, L. Magtanong, B. Ford, P.H. Tang, M.A. Roberts, B. Tong, T.J. Maimone, R. Zoncu, M.C. Bassik, D.K. Nomura, S.J. Dixon, J. A. Olzmann, The CoQ oxidoreductase FSP1 acts parallel to GPX4 to inhibit ferroptosis, Nature 575 (2019) 688–692, https://doi.org/10.1038/s41586-019-1705-2.

[32] Y. Yuan, Y. Zhai, J. Chen, X. Xu, H. Wang, Kaempferol ameliorates oxygen-glucose deprivation/reoxygenation-induced neuronal ferroptosis by activating nrf2/slc7a11/GPX4 Axis, Biomolecules 11 (2021) 923, https://doi.org/10.3390/biom11070923.

[33] N.P. Committee, Pharmacopoeia of the People's Republic of China, Partisans 1 (2015) 188–189.

[34] X. Yan, Q. Zhang, F. Feng, Chemical profiling approach to evaluate the influence of traditional and simplified decoction methods on the holistic quality of Da-Huang-Xiao-Shi decoction using high-performance liquid chromatography coupled with diode-array detection and time-of-flight mass spectrometry, J. Separ. Sci. 39 (2016) 1442–1453, https://doi.org/10.1002/jssc.201501326.

[35] X. Zhou, J. Yang, Y. Liu, Z. Li, J. Yu, W. Wei, Q. Chen, C. Li, N. Tang, Observation of the effect of bone marrow mesenchymal stem cell transplantation by different interventions on cirrhotic rats, Braz. J. Med. Biol. Res. 52 (2019) e7879, https://doi.org/10.1590/1414-431X20187879.

[36] H. Wang, T. Li, H. Xiang, X. Zhang, K. Fang, G. Wu, M. Yan, N. Xue, M. Chen, T. Xie, Y. Zhang, P. Wang, H. Lei, Origin and formation mechanism investigation of compound precipitation from the traditional Chinese prescription huang-lian-jie-du-tang by isothermal titration calorimetry, Molecules 22 (2017) 1456, https://doi.org/10.3390/molecules22091456.

[37] X. Xu, H. Xu, Y. Shang, R. Zhu, X. Hong, Z. Song, Z. Yang, Development of the general chapters of the Chinese Pharmacopoeia 2020 edition: a review, J Pharm Anal 11 (2021) 398–404, https://doi.org/10.1016/j.jpha.2021.05.001.

[38] A.B. Nair, S. Jacob, A simple practice guide for dose conversion between animals and human, J. Basic Clin. Pharm. 7 (2016) 27–31, https://doi.org/10.4103/0976-0105.177703.

[39] J. Zhou, J. Pan, Z. Xiang, Q. Wang, Q. Tong, J. Fang, L. Wan, J. Chen, Data on the optimization of the formula of Xiaokeyinshui extract combination treating diabetes mellitus using uniform experimental design in mice, Data Brief 32 (2020), 106134, https://doi.org/10.1016/j.dib.2020.106134.

[40] J. Chen, L. Wang, H. Xu, L. Xing, Z. Zhuang, Y. Zheng, X. Li, C. Wang, S. Chen, Z. Guo, Q. Liang, Y. Wang, Meningeal lymphatics clear erythrocytes that arise from subarachnoid hemorrhage, Nat. Commun. 11 (2020) 3159, https://doi.org/10.1038/s41467-020-16851-z.

[41] P.A. Campochiaro, T.A. Mir, The mechanism of cone cell death in Retinitis Pigmentosa, Prog. Retin. Eye Res. 62 (2018) 24–37, https://doi.org/10.1016/j.preteyeres.2017.08.004.

[42] F. Liu, X. Liu, Y. Zhou, Y. Yu, K. Wang, Z. Zhou, H. Gao, K.-F. So, N. Vardi, Y. Xu, Wolfberry-derived zeaxanthin dipalmitate delays retinal degeneration in a mouse model of retinitis pigmentosa through modulating STAT3, CCL2 and MAPK pathways, J. Neurochem. 158 (2021) 1131–1150, https://doi.org/10.1111/jnc.15472.
[43] L. Tang, S. Bao, Y. Du, Z. Jiang, A.O. Wuliji, X. Ren, C. Zhang, H. Chu, L. Kong, H. Ma, Antioxidant effects of Lycium barbarum polysaccharides on photoreceptor degeneration in the light-exposed mouse retina, Biomed. Pharmacother. 103 (2018) 829–837, https://doi.org/10.1016/j.biopha.2018.04.104.
[44] Y. Ma, R. Kawasaki, L.P. Dobson, J.B. Ruddle, L.S. Kearns, T.Y. Wong, D.A. Mackey, Quantitative analysis of retinal vessel attenuation in eyes with retinitis pigmentosa, Invest. Ophthalmol. Vis. Sci. 53 (2012) 4306–4314, https://doi.org/10.1167/iovs.11-8596.
[45] Z. Jiang, W. Gao, L. Huang, Tanshinones, critical pharmacological components in Salvia miltiorrhiza, Front. Pharmacol. 10 (2019) 202, https://doi.org/10.3389/fphar.2019.00202.
[46] Y. Li, E.D. Cohen, H. Qian, Rod and cone coupling modulates photopic ERG responses in the mouse retina, Front. Cell. Neurosci. 14 (2020), 566712, https://doi.org/10.3389/fncel.2020.566712.
[47] M. Lang, A. Harris, T.A. Ciulla, B. Siesky, P. Patel, A. Belamkar, S. Mathew, A.C. Verticchio Vercellin, Vascular dysfunction in retinitis pigmentosa, Acta Ophthalmol. 97 (2019) 660–664, https://doi.org/10.1111/aos.14138.
[48] D.-Y. Li, Q. Xia, T.-T. Yu, J.-T. Zhu, D. Zhu, Transmissive-detected laser speckle contrast imaging for blood flow monitoring in thick tissue: from Monte Carlo simulation to experimental demonstration, Light Sci. Appl. 10 (2021) 241, https://doi.org/10.1038/s41377-021-00682-8.
[49] E. Deleon, M. Lederman, E. Berenstein, T. Meir, M. Chevion, I. Chowers, Alteration in iron metabolism during retinal degeneration in rd10 mouse, Invest. Ophthalmol. Vis. Sci. 50 (2009) 1360–1365, https://doi.org/10.1167/iovs.08-1856.
[50] Z. Tang, Y. Ju, X. Dai, N. Ni, Y. Liu, D. Zhang, H. Gao, H. Sun, J. Zhang, P. Gu, HO-1-mediated ferroptosis as a target for protection against retinal pigment epithelium degeneration, Redox Biol. 43 (2021), 101971, https://doi.org/10.1016/j.redox.2021.101971.
[51] B.S. Rogers, R.C.A. Symons, K. Komeima, J. Shen, W. Xiao, M.E. Swaim, Y.Y. Gong, S. Kachi, P.A. Campochiaro, Differential sensitivity of cones to iron-mediated oxidative damage, Invest. Ophthalmol. Vis. Sci. 48 (2007) 438–445, https://doi.org/10.1167/iovs.06-0528.
[52] W. Shu, B.H. Baumann, Y. Song, Y. Liu, X. Wu, J.L. Dunaief, Ferrous but not ferric iron sulfate kills photoreceptors and induces photoreceptor-dependent RPE autofluorescence, Redox Biol. 34 (2020), 101469, https://doi.org/10.1016/j.redox.2020.101469.
[53] G.E.O. Borgstahl, R.E. Oberley-Deegan, Superoxide dismutases (SODs) and SOD mimetics, Antioxidants 7 (2018) 156, https://doi.org/10.3390/antiox7110156.
[54] F. Ursini, M. Maiorino, Lipid peroxidation and ferroptosis: the role of GSH and GPx4, Free Radic. Biol. Med. 152 (2020) 175–185, https://doi.org/10.1016/j.freeradbiomed.2020.02.027.
[55] X. Y, L. Y, L. J, C. W, Ethyl carbamate triggers ferroptosis in liver through inhibiting GSH synthesis and suppressing Nrf2 activation, Redox Biol. 53 (2022), https://doi.org/10.1016/j.redox.2022.102349.
[56] C. Wang, S. Chen, H. Guo, H. Jiang, H. Liu, H. Fu, D. Wang, Forsythoside A mitigates alzheimer's-like pathology by inhibiting ferroptosis-mediated neuroinflammation via nrf2/GPX4 Axis activation, Int. J. Biol. Sci. 18 (2022) 2075–2090, https://doi.org/10.7150/ijbs.69714.
[57] J. Liu, G. Yang, H. Zhang, Glyphosate-triggered hepatocyte ferroptosis via suppressing Nrf2/GSH/GPX4 axis exacerbates hepatotoxicity, Sci. Total Environ. 862 (2023), 160839, https://doi.org/10.1016/j.scitotenv.2022.160839.
[58] W.S. Yang, R. SriRamaratnam, M.E. Welsch, K. Shimada, R. Skouta, V.S. Viswanathan, J.H. Cheah, P.A. Clemons, A.F. Shamji, C.B. Clish, L.M. Brown, A. W. Girotti, V.W. Cornish, S.L. Schreiber, B.R. Stockwell, Regulation of ferroptotic cancer cell death by GPX4, Cell 156 (2014) 317–331, https://doi.org/10.1016/j.cell.2013.12.010.